Int. J. Electrochem. Sci., 17 **(2022)** Article Number: 220557, doi: 10.20964/2022.05.54

International Journal of ELECTROCHEMICAL SCIENCE
www.electrochemsci.org

Synergistic Enhancement of Photoelectric Performance of TiO_2 Photoanodes through Polyoxometalate and Blue Honeysuckle (*Lonicera caerulea* L.) Anthocyanins

Shuyuan Wang[1], *Chunqing Mi*[1], *Lihao Wang*[1,*], *Qian Tang*[2], *Hongyu Cao*[2], *Xuefang Zheng*[2,*]

[1] College of Environmental and Chemical Engineering, Dalian University, Dalian116622, China
[2] College of Life Science and Technology, Dalian University, Dalian116622, China
[*]E-mail: wanglh132@163.com;dlxfzheng@126.com
Shuyuan Wang and Chunqing Mi contributed equally to this work.

Received: 20 November 2021/ *Accepted:* 24 January 2022 / *Published:* 5 April 2022

In this work, natural Lonicera eduli anthocyanins (the main component is cyanidin 3-O-glucoside,abbr. C3G) and Dawson-type polyoxometalate $K_6P_2W_{18}O_{62}$,abbreviated P_2W_{18}, were introduced into a TiO_2 photoanode to produce a synergistic effectfor the first time. It can have a synergistic effect that enhances the photovoltaic and photoelectrocatalytic performancesof the TiO_2 photoanode. We fabricated multilayer film photoanodes by the layer-by-layer(LbL) assembly method. Experimental resultsprove thatthe P_2W_{18}/TiO_2/C3G filmpossess a better photocurrent response and higher power conversion efficiency than TiO_2films, G3G/TiO_2films and P_2W_{18}/TiO_2 films alone. Meanwhile, the P_2W_{18}/TiO_2/C3G film also displayed higherphotoelectrocatalytic activity for methanol than the other films. These resultscanprovideimportantinformation for photovoltaic and electrochemical sensors.

Keywords: Blue honeysuckleanthocyanins; Titanium dioxide; Composite film; Photoelectric performance; Dawson-type polyoxometalate

1. INTRODUCTION

With the acceleration of fossil energy consumption, the development and utilization of solar energy is increasingly the focus of international attention [1,2].Dye sensitized solar cell (DSSC) is a common photoelectric converter with high photoelectric conversion efficiency and low cost and it is a research hotspot. [3].As a photoanode material in DSSCs, $TiO_2$is the most widely used semiconductor due to its inherent photoelectric conversion property, high chemical stability, and low cost[4]. Meanwhile,theapplication of wide-band-gap (3.2 eV) $TiO_2$is safe [4].However, in practical application, the photoelectric conversion efficiency of TiO_2 is too low. Combined with previous reports, we believe that this phenomenon is due to it has high electron hole recombination rate[5]. Various strategies have been used to increase the absorption wavelength and carrier mobility, such as modification of metals

and doping agents [6-7]. TiO_2 can also be combined with other materials [8], specifically,graphene [9], CdTe and CdS nanocrystals [10], Bi_2S_3-BiOBr nanosheets [11], ZrO_2 [12],and Sb_2S_3 [13].

Polyoxometalates (POMs) are metal-oxygen nanoclusters with various chemical compositions and structures, and they also haveexcellent redox and photoelectrochemical properties [14-15].POMs can acceptelectronsto increasetheelectron transfer rate of the TiO_2 trapping photogenerated electrons, so they can effectively prove the photoelectrochemical performance ofthe semiconductor. It is an effective strategy to introduce POMs into semiconductors to preventfast electron-hole recombination.

Anthocyanin is a natural pigment with strong heat and light resistancethat is widely found in fruit pulp. It is a flavonoid compound, and the absorption wavelengths of anthocyanins are approximately 280 nm and 500~550 nm, respectively. Among more than 500 kinds of natural anthocyanins, 3-O-glucoside anthocyanins are the most abundant and representative because of their advantages of good stability, low cost and environmental friendliness [16-17]. It can be used as an excellent natural sensitizer for DSSCs by expanding the excitation wavelength of semiconductors [18-19].

To summarise, P_2W_{18}hasgreat electron-hole separation efficiencyand the effective expansion of the excitation wavelength of semiconductors from anthocyanins, wepreparedternary nanocomposite film photoanodes consisting of TiO_2 nanoparticles, P_2W_{18} and G3G. The P_2W_{18}/TiO_2/C3G films were obtained bythe layer-by-layer(LbL) assembly technique. and itcan be demonstrated that they hadthe highest photocurrent and conversion efficiency compared tothe only TiO_2 film, the G3G/TiO_2 film and the P_2W_{18}/TiO_2 film.In order to further study the photocatalytic performance of composite films electrodes, methanol was selected as the object of photocatalytic oxidation. All these results provideimportantreference material for DSSCs and electrochemical sensors.

2. EXPERIMENT

2.1.Reagents and chemicals

TiO_2 and $K_6P_2W_{18}O_{62}$ were synthesizedby referencingliteratures [20-21].The synthesized method and characterization of TiO_2 and $K_6P_2W_{18}O_{62}$were shown in Fig.S1.

Lonicera eduli anthocyanins (40 wt% cyanidin 3-O-glucoside) were provided by Northeast Forestry University. 3-Aminopropyltrimethoxysilane,abbreviated APS, and poly(allylamine hydrochloride) (PAH) were producedby Aldrich. Poly(styrenesulfonate),abbreviated PSS,was purchased from Beijing Bailingwei Technology Co., Ltd. All of chemicalswere AR grade and deionized water was used in this work.

2.2.Deposition of the LbL assemblyfilms

ITO-coated glass was cleaned before the layer-by-layer (LbL) assembly process by the literaturemethods [22].After cleaning the indium-tin oxide (ITO) electrodes were immersedin APS solutionat leastall night, and the next step is put themin HCl (pH 2) solution for about 20 min. Then, put substratesinto the P_2W_{18} (2×10^{-3} M, pH1.5), TiO_2 solution, C3G (1.0 $g\cdot L^{-1}$) and the PAH (4 $g\cdot L^{-1}$)

for10 min, 1 min, 10 min and 10 min.The samples were flushed and dried after put them into solution. The operation steps were repeatedto prepare $(P_2W_{18}/TiO_2/C3G/PAH)_2$ films, which were dried at room temperature for12h. For comparison, $(PSS/TiO_2)_2$ films, $(C3G/TiO_2)_2$ films and $(P_2W_{18}/TiO_2)_2$ films were obtainedusinga homologous method.

2.3. characterizationof the films

UV–visabsorption spectrawereobtained bya UV-2600 UV–visible spectrophotometer. XPS spectra were recorded on ESCALAB 250 Surface Analysis System. IR spectra were recorded on a Magna-550IIInfrared spectrometer. AFM measurements were obtained by a Nanoscope V Multimode 8 Probe Station. The light sourcewas a 300 W Xe lamp with alight intensity of 6.7×10^2 μW·cm^{-2}and a wavelength range of 320∼780 nm. A Shanghai ChenhuaCHI660E Electrochemical Workstation was used to record photoelectrochemical experimentswith a custom three-electrode system at room temperature. The reference electrode was a saturated calomel electrode, a platinum wire was used as the counter electrode, and the working electrodewasa composite filmdeposited on ITO glass.The actualarea ofthe working electrode was about 1.5cm^2. Na_2SO_4 solution (0.1 M) was electrolyte.

3. RESULTS AND DISCUSSION

3.1. Characterization of the lonicera eduli anthocyanins

UV–vis absorption spectra confirmed the characteristic bands of Lonicera eduli anthocyanins at280 nm, 325nmand 518 nmwas seen in Fig.1A. IR spectra ofLonicera eduli anthocyaninsare exhibited in Fig.1B.

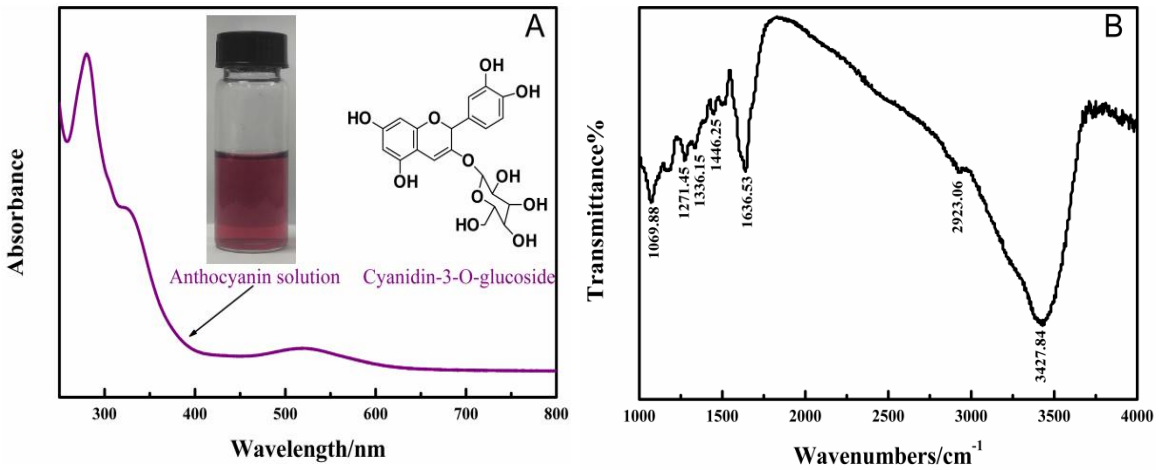

Figure 1. (A) UV–visspectra of C3G;(B) IR spectra of C3G

Meanwhile, the absorption peak at 3427.84 cm^{-1} corresponded to many O-H stretching vibration peaks of aromatic rings and glycosylsdue to the structure of C3G.The peak at 2923.06 cm^{-1} in

the spectrogram appeared due to methylene stretching vibrations in the glycosyl. It is clear that the absorption peaks at 1636.53 cm^{-1} and 1446.25 cm^{-1}werebased on the aromatic and heterocyclic ring skeletalvibrations in the chromene of C3G. The absorption peaks at 1336.15 cm^{-1}, 127145cm^{-1} and 1069.88 cm^{-1} corresponded to the stretching vibration of C-O in glycosyl [23].

3.2. UV–vis absorption spectra of the composite film electrode

Negatively charged P_2W_{18} and C3G and positively charged TiO_2 and PAH can adsorb toeach otherdue to the Coulomb force.UV–vis spectroscopy was employed to observe the absorption process of thesamples.The composite films were depositedon a quartz substrate. As shown Fig.2, in the UV region, the characteristic absorption bands of TiO_2 and P_2W_{18}can be observed at 248 nm, 201 nm and 295 nm, respectively. Meanwhile, it is easy to observe the absorption processwith the growth of films.The absorption bands of C3G were not observed at 280 nm and 325 nm because they were covered by the ultraviolet absorption region of TiO_2. The characteristic peak of C3Gappeared at 560 nm, and it was redshifted by 42 nm from the original visible absorption peak of 518 nm. The reason is that the aromatic hydroxyl groups of natural dyes chemically adsorb on the surface of TiO_2 and chelate with Ti(IV) ions [24-26].The schematic of cyanidin 3-O-glucoside adsorption on the surface of TiO_2(Fig.S2 in ESI).This figureindicates that the $(P_2W_{18}/TiO_2/C3G/PAH)_2$ films were prepared uniformly and homogeneously.

Meanwhile, the UV–vis absorption spectraalsoshow information about the amount of TiO_2(Fig.S3~S5 in ESI).We can use the equation ($\Gamma = N_A A_{n\lambda TiO2}/2n\epsilon_\lambda$[27]) to calculate the surface coverage (Γ) of TiO_2 on samples. Specifically,$A_{n\lambda TiO2}$ ($A_{n\lambda TiO2} = A_{n\lambda total}$-$A_{n\lambda P2W18}$, $n \geq 1$) is the absorbance of TiO_2 at a given wavelength (λ=248 nm).Through the calculation of the formula, we got the information about the proportion of the surface coverage of TiO_2 in Table 1.

Table 1. The ratio of the surface coverage of TiO_2

the ratio of the surface coverage of TiO_2 between different two films	ratio
the $(P_2W_{18}/TiO_2)_2$film : the $(PSS/TiO_2)_2$ film	1.01:1.00
the $(P_2W_{18}/TiO_2)_2$film : the $(P_2W_{18}/TiO_2/C3G/PAH)_2$ film	1.07:1.00
the $(P_2W_{18}/TiO_2)_2$ film: the $(C3G/TiO_2)_2$ film	1.01:1.00

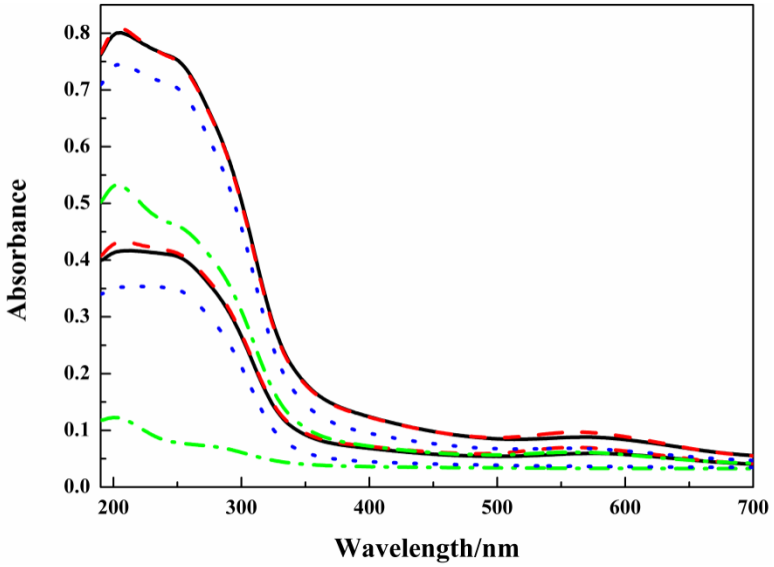

Figure 2. UV–vis absorption spectra of the film $(P_2W_{18}/TiO_2/C3G/PAH)_2$.The dashed-dotted line, dotted line, dotted line and solid line indicate spectras after P_2W_{18} deposition, TiO_2 deposition, C3G deposition and PAH deposition, respectively.

3.3. X-ray photoelectron spectrum (XPS)

While the $(P_2W_{18}/TiO_2/C3G/PAH)_2$ film was deposited on silicon substrates,the chemical composition and the binding energy of this film can be provided by XPS spectra.We can determine that these elements exist in the $(P_2W_{18}/TiO_2/C3G/PAH)_2$ film by observing the peaks of P, W, Ti and O in the Fig.3.The peaks of W 4f and P 2pappeared at 35.2, 37.2 and 133 eV, giving an approximate expected atom ratio of P_2W_{18}in quantitation [28].We dissolved anthocyanins in a PSS solution to make them negatively chargedwhile preparing the $(P_2W_{18}/TiO_2/C3G/PAH)_2$ film.To ensure that the anthocyanins can be successfully assembled into a film, we prepared $(P_2W_{18}/TiO_2/C3G/PAH)_2$ film and $(P_2W_{18}/TiO_2/PSS/PAH)_2$ film to observe the changes in their bond positions.XPS spectra of theTi 2p and O 1 s regions (Fig.3C and 3D) of the $(P_2W_{18}/TiO_2/C3G/PAH)_2$ film and the $(P_2W_{18}/TiO_2/PSS/PAH)_2$ film. The Ti $2p_{3/2}$ binding energy values of the $(P_2W_{18}/TiO_2/C3G/PAH)_2$ film and the $(P_2W_{18}/TiO_2/PSS/PAH)_2$ film are found to be 458.0 and 458.3 eV, respectively. The peak of the $(P_2W_{18}/TiO_2)_2$ film is shifted by 0.3 eV compared to the $(P_2W_{18}/TiO_2/C3G/PAH)_2$ film.The O 1 s peaks are recorded at 529.3, 531.5 and 532.7 eV, corresponding to Ti-O-Ti, Ti-OH and C-O-Ti [29].These data show thatcyanidin 3-O-glucoside is chemically adsorbed on the surface of TiO_2 through the hydroxyl group, replacing the Ti-O-Ti bond in $TiO_2$and finally forming Ti-O-C and Ti-OH bonds [30]. The abovedatasconfirm that P_2W_{18}, TiO_2 and C3G are depositedinto the $(P_2W_{18}/TiO_2/C3G/PAH)_2$ film.

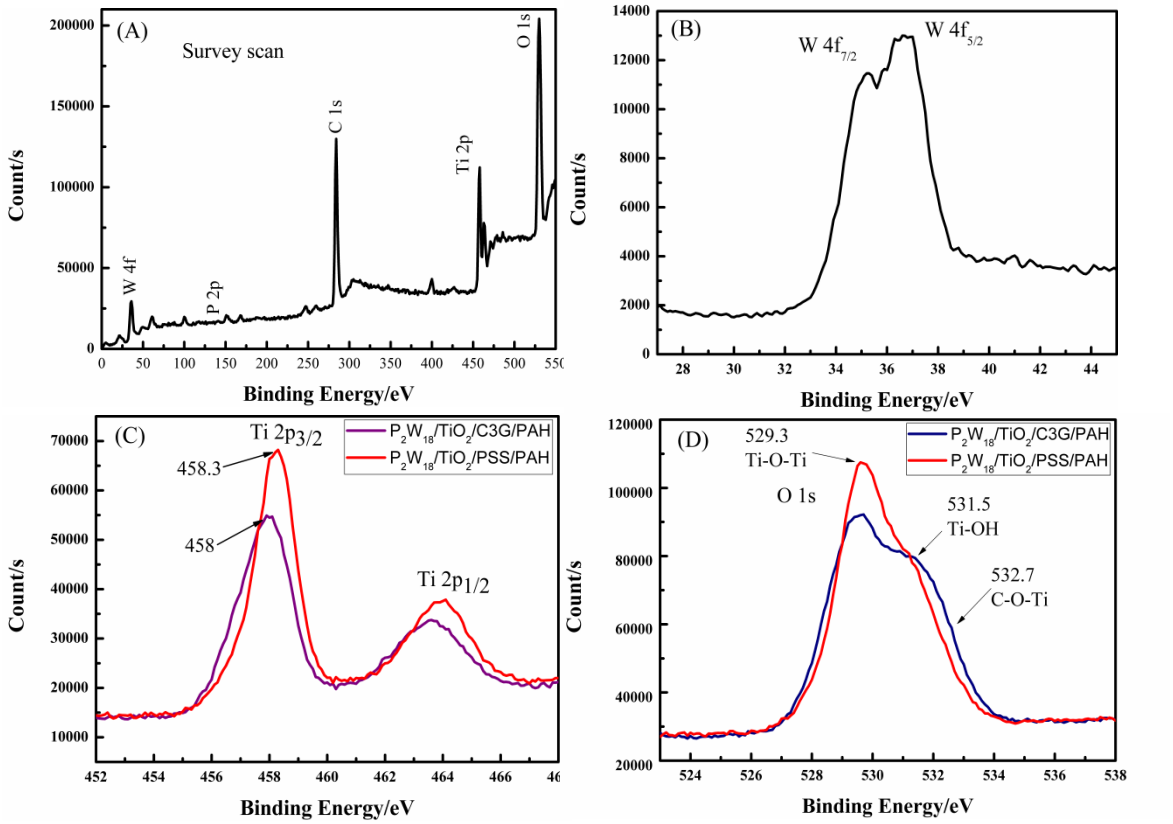

Figure 3. XPS spectra of the $(P_2W_{18}/TiO_2/C3G/PAH)_2$ film. (A)Survey scan; (B)W; (C)Ti; (D)O.

3.4. Investigation of surface morphology

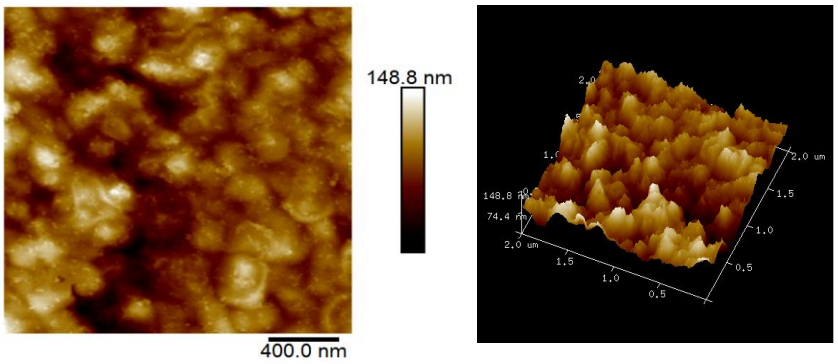

Figure 4. AFM picture of the $(P_2W_{18}/TiO_2/C3G/PAH)_2$film on the silicon wafer.

AFM was used to observesurface morphology and homogeneity of the composite films. The AFM picture of the $(P_2W_{18}/TiO_2/C3G/PAH)_2$ film was shown in Fig.4.The sample exhibits spherical and granular morphologic features because it is mainly formed by the electrostatic effect of various particles with different electrical properties gathered together [3, 31-32]. According to Fig.4,the average size of spherical particles is approximately 106 nm, the surface roughness is 10.3 nm, and the thickness of the $(P_2W_{18}/TiO_2/C3G/PAH)_2$film is approximately 123.5 nm. Meanwhile,the AFM three-dimensional image shows that the multilayer film has a good distribution state.

3.5.Photocurrent versus time (I-T)curves

Our research focuses on the photoelectrochemical properties of the composite films. The electrolyte used in the experiment is 0.1M Na_2SO_4 solution. The whole process was illuminated by xenon lampand the set bias voltage was 0.1V.Fig.5 displays the anodic photocurrent responses ofthe $(P_2W_{18}/TiO_2/C3G/PAH)_n$ (n =1-3) films. We can observed that the steady-state photocurrent were increasing gradually with the increase of the number of composite film layers. And it should be noted that when the number of composite film layers was 2, the photocurrent response was the largest.Above phenomenon can be interpreted as more TiO_2 nanoparticles and anthocyanins can absorb sunlight to make more photogenerated carriers.However,due to the electron transfer rates of the composite films to the ITO-glassesis slow whenthe number of layers increases [33], the photocurrent of the $(P_2W_{18}/TiO_2/C3G/PAH)_3$ film islower than that of the $(P_2W_{18}/TiO_2/C3G/PAH)_2$ film.In summary, the optimal number of $P_2W_{18}/TiO_2/C3G/PAH$ composite films was 2 layers.

Fig.6 displays the photocurrent changes of (a) the $(PSS/TiO_2)_2$ film, (b) the $(C3G/TiO_2)_2$film, (c) the $(P_2W_{18}/TiO_2)_2$ film, and (d) the $(P_2W_{18}/TiO_2/C3G/PAH)_2$ film. This part of the experiment was carried out with the X-lamp turned on and off every 30 seconds while all of the composite films exhibit fast and stablephotocurrent response. Thecompositefilms exhibitfast anodic photocurrent responses. By comparison, the photocurrent of the $(P_2W_{18}/TiO_2/C3G/PAH)_2$ filmwas higher thanthat of the$(PSS/TiO_2)_2$ film, the $(C3G/TiO_2)_2$ film and the $(P_2W_{18}/TiO_2)_2$ film. All above results indicatethatP_2W_{18}can as an efficient electron acceptor to enhance the inherent photocurrent response of TiO_2. Meanwhile,anthocyanins were used to increase the photocurrent for the standout photosensitizing performance[34].

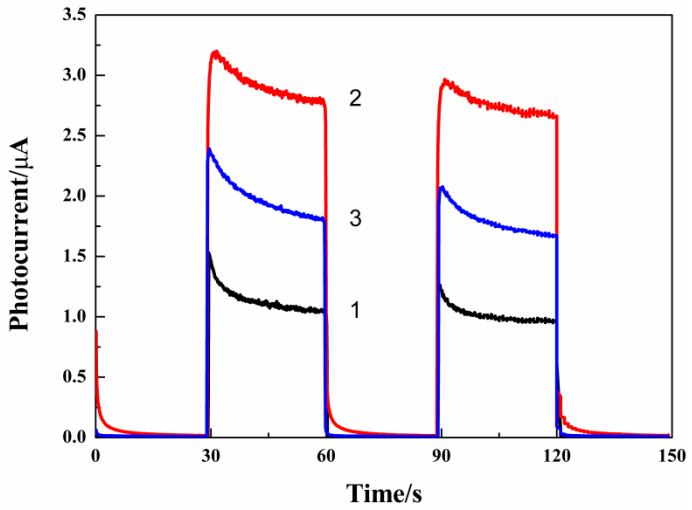

Figure 5. *I-T*curves of the $(P_2W_{18}/TiO_2/C3G/PAH)_n$ films (n =1-3).

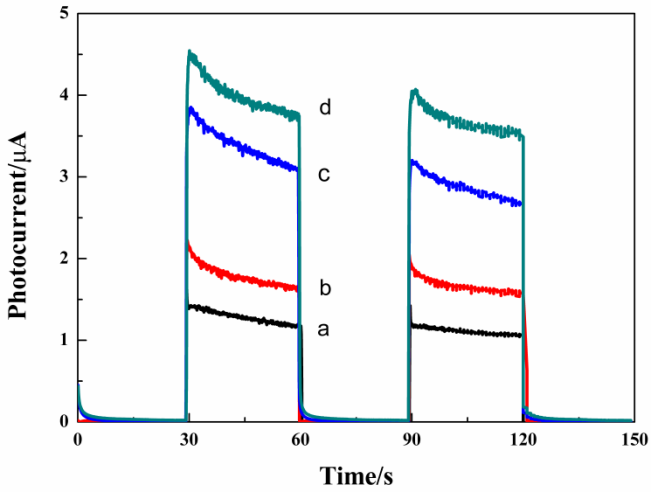

Figure 6. *I-T* curves: (a) the $(PSS/TiO_2)_2$ film, (b) the $(C3G/TiO_2)_2$film, (c) the $(P_2W_{18}/TiO_2)_2$ film and (d) the $(P_2W_{18}/TiO_2/C3G/PAH)_2$ film.

3.6. Current-voltage (I-V) Curves

The Current-voltage (*I-V*) Curves can be used to investigate the photoelectron conversion efficiency of the different composite films. As shown in Fig.7, the *I-V*curves of (a) the $(PSS/TiO_2)_2$ film, (b) the $(C3G/TiO_2)_2$film, (c) the $(P_2W_{18}/TiO_2)_2$ film and (d) the $(P_2W_{18}/TiO_2/C3G/PAH)_2$ film were obtained under Xe lamp irradiation.The corresponding photovoltaic parameters of all the multilayer films are calculated and listed in Table 2. The intersections of the curves with the abscissa and ordinate represents the open circuit voltage and short-circuit current, respectively.Formulas ($ff = (J_{max}V_{max})/(J_{sc}V_{oc})$, $\eta = P_{out}/P_{in} = ff\ (J_{sc}V_{oc})/P_{in}$)were used to calculate fill factor (*ff*) and power conversion efficiency (η,%).

Evidently, the $(P_2W_{18}/TiO_2/C3G/PAH)_2$ film shows the highest power conversion efficiency among the four kinds of films, corresponding tothe data of the above *I-V*curvesexperiments. According to the test data of the *I-V* curve, the power conversion efficiency of the$(C3G/TiO_2)_2$ film has a small improvement thanthat of the$(PSS/TiO_2)_2$ filmby comparison. Because cyanidin 3-O-glucoside provides a large number of photogenerated electrons during the sensitization process, the photogenerated electrons cannot be transported out and recombined with the holes of TiO_2.When polyoxometalate is introduced, the power conversion efficiency of the multilayer film issignificantly improved. Thus,the combination of P_2W_{18} and C3G into TiO_2 could significantly improve the photoelectric performance of TiO_2.

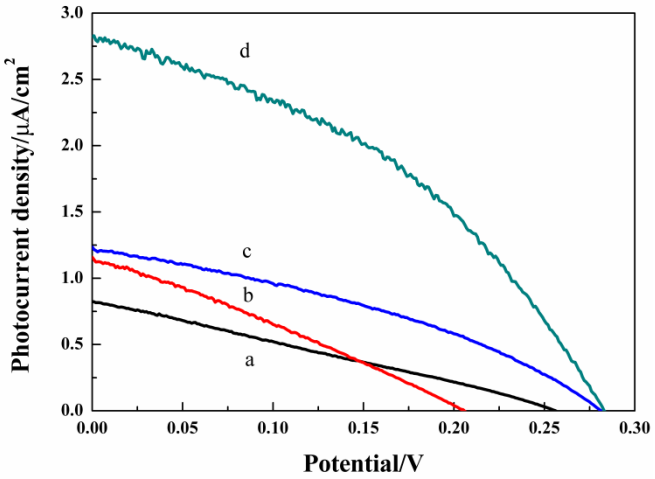

Figure 7. *I-V* curves:(a) the $(PSS/TiO_2)_2$ film, (b) the $(C3G/TiO_2)_2$film, (c) the $(P_2W_{18}/TiO_2)_2$ film,and (d) the $(P_2W_{18}/TiO_2/C3G/PAH)_2$ film.

Table 2. Photovoltaic parameters of the multilayer films.

	P_{max}(μW)	J_{sc}(μA▪cm^2)	V_{oc}(V)	*FF*	*η*(%)
$(PSS/TiO_2)_2$	0.0557	0.80	0.26	0.27	0.0083
$(C3G/TiO_2)_2$	0.0665	1.15	0.21	0.28	0.0099
$(P_2W_{18}/TiO_2)_2$	0.1227	1.20	0.28	0.37	0.0183
$(P_2W_{18}/TiO_2/C3G/PAH)_2$	0.3163	2.80	0.28	0.40	0.0472

According to the above data, the mechanism diagramof electron transfer processes is proposed in Fig.8. The redox potentials of $K_6P_2W_{18}O_{62}$, TiO_2 and C3G are +0.34 V, -0.5 V and -1.17 V, respectively [36,37]. First, C3G and TiO_2 absorb light to generate photogenerated electrons, and the photogenerated electrons generated by C3G migrate from the LUMO to the CB of TiO_2. Second, the photoinduced electrons transfer from the CB of TiO_2 into the LUMO of $K_6P_2W_{18}O_{62}$. The photoinduced electrons transfer from $K_6P_2W_{18}O_{62}$ to indium-tin oxide (ITO) electrodes and finally to the external circuit [38]. At the same time, the excited C3G and the holes of TiO_2 migrate to the photoanode-electrolyte interface, and the electrolyte provides electrons to complete the photogenerated electron transfer. In the whole process, C3G acts as a photoactive material to sensitize TiO_2 and extend the excitation wavelength of TiO_2 to improve light utilization. P_2W_{18} acts as an electron acceptor to extend the recombination time of photogenerated electrons and holes.Under their joint action, the photovoltaic performance of the multilayer film photoanode increases.

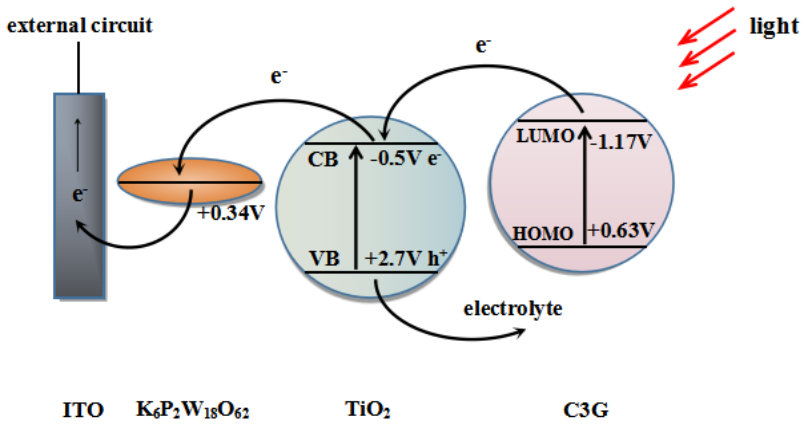

Figure 8. Mechanismdiagram describingthe electron transfer pathways in the $(P_2W_{18}/TiO_2/C3G/PAH)_2$film photoanode.

3.7.Oxidation of methanol with the composite films electrodes

We supposed the photoelectronoxidation process of methanol can be used to observe the photoelectrocatalytic activity of the composite films. This part of the experiment was carried out at a constant bias of 0.1 V vs Hg/Hg_2Cl_2 and 0.1 Mneutralphosphate buffer solution (pH 7) as electrolyte. Fig.9 (A) displays the photocurrents done for (a) the $(P_2W_{18}/TiO_2/C3G/PAH)_2$ film, (b) the $(P_2W_{18}/TiO_2)_2$ film, (c) the $(C3G/TiO_2)_2$film, and (d) the $(PSS/TiO_2)_2$ film in different concentrations of methanolwhen the Xe lamp is switched on. It is clear that the $(P_2W_{18}/TiO_2/C3G/PAH)_2$compositefilm shows the highest photocurrentresponsein the range (0.05 M-0.25 M)of methanol.

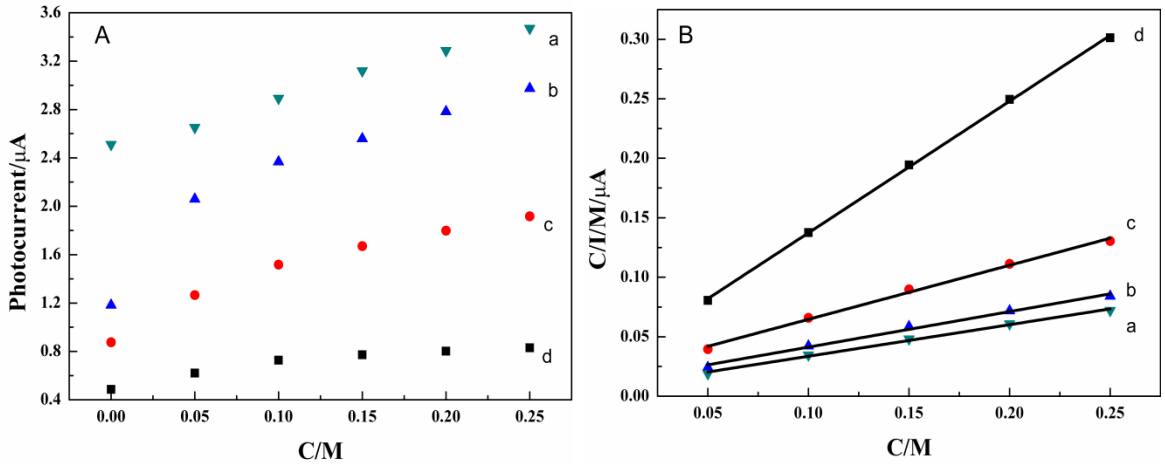

Figure 9. (A) Relationship between photocurrent and methanol concentration of (a) the $(P_2W_{18}/TiO_2/C3G/PAH)_2$ film, (b) the $(P_2W_{18}/TiO_2)_2$ film, (c) the $(C3G/TiO_2)_2$film, and(d) the $(PSS/TiO_2)_2$ film; (B) Plot of *C*/*I*vs *C* for (a) the $(P_2W_{18}/TiO_2/C3G/PAH)_2$ film, (b) the $(P_2W_{18}/TiO_2)_2$ film, (c) the $(C3G/TiO_2)_2$film, and(d) the $(PSS/TiO_2)_2$ film.

This indicates that the $(P_2W_{18}/TiO_2/C3G/PAH)_2$ film has a betterphotoelectrochemical oxidation activity for methanol. It can be seen from the principle of photoelectric catalysis that TiO_2 mainly relies on holes to directly oxidize methanol or electrons react with hydroxide in water to generate hydroxyl radical reoxidized methanol. Direct hole transfer leaded to the increase in the photocurrent measuredcurrent during the test.Above conclusionis alikewith the datas of Maruga ´n and coworkers [39].When the thin filmswere the working electrodes to oxidize methanol, the kinetic curve between concentration/photocurrent (*C/I*) and methanol concentration (linearly in the 0.05-0.25 M range)was shown in Fig. 9 (B). Specifically, (a) was the $(P_2W_{18}/TiO_2/C3G/PAH)_2$ film, (b) was the $(P_2W_{18}/TiO_2)_2$ film, (c) was the $(C3G/TiO_2)_2$film and (d) was the $(PSS/TiO_2)_2$ film on this plot. Meanwhile, the results also abides bythe Langmuir-Hinselwood kinetics equation [40].

4. CONCLUSION

The$P_2W_{18}/TiO_2/C3G$ films were prepared first by the LbLassembly method. Photoelectric performance tests showed that the $(P_2W_{18}/TiO_2/C3G/PAH)_2$film exhibited a higher photocurrent and power conversion efficiency than the$(P_2W_{18}/TiO_2)_2$ film and the $(PSS/TiO_2)_2$ film.It can be attributed tothe advancement of electro-hole separation efficiency by P_2W_{18} and the expansion of the excitation wavelength of semiconductors by anthocyanins. On the other hand, the $P_2W_{18}/TiO_2/C3G$ film also has good photoelectrochemical oxidation activity for methanol.This article fullydemonstrates the synergistic effect and that the Dawson-type polyoxometalate and anthocyanins couldimprovethe photovoltaic performance of $TiO_2$for the first time. Meanwhile, this work is potentially useful for photovoltaics, solar cells, electrochemical sensors and so on.

ACKNOWLEDGMENTS
The authors are grateful for the financial support from the Natural Science Foundation of China (Grant No. 21601023, 21601024 and 21601025) and the Dalian Youth Science and Technology Star Project (Grant No. 2018RQ63).

CONFLICT OF INTERESTS
"The authors declare that there are no conflicts of interest regarding the publication of this article."

SUPPORTING INFORMATION

Preparation of $K_6P_2W_{18}O_{62}$: $Na_2WO_4{\cdot}2H_2O$ (20 g) was added to 70 mL of water, and the solution was heated to boiling. Then, 30 mL of 85% H_3PO_4 was slowly added to the boiling solution, and the resulting yellow–green solution was refluxed for 5-13 h. The solution was cooled, and the product was precipitated byadding 20 g of solid KCl. The light green precipitate was collected, redissolved in a minimum amount of hot water, and allowed to crystallize at 5 °C overnight [41].

Preparation of TiO_2colloidal solution: Put 95% isopropyl titanate (10 mL) and isobutanol (1.6 mL) in a beaker and mix evenly at room temperature.In the process of magnetic stirring, slowly add dropwise to the round bottom flask, put in distilled water (60 mL) in a dropper, and then add concentrated nitric acid (0.42 mL) during the reaction.The reaction was stirred at 80 °C for8h to obtain a stable milky white TiO_2 colloidal solution.

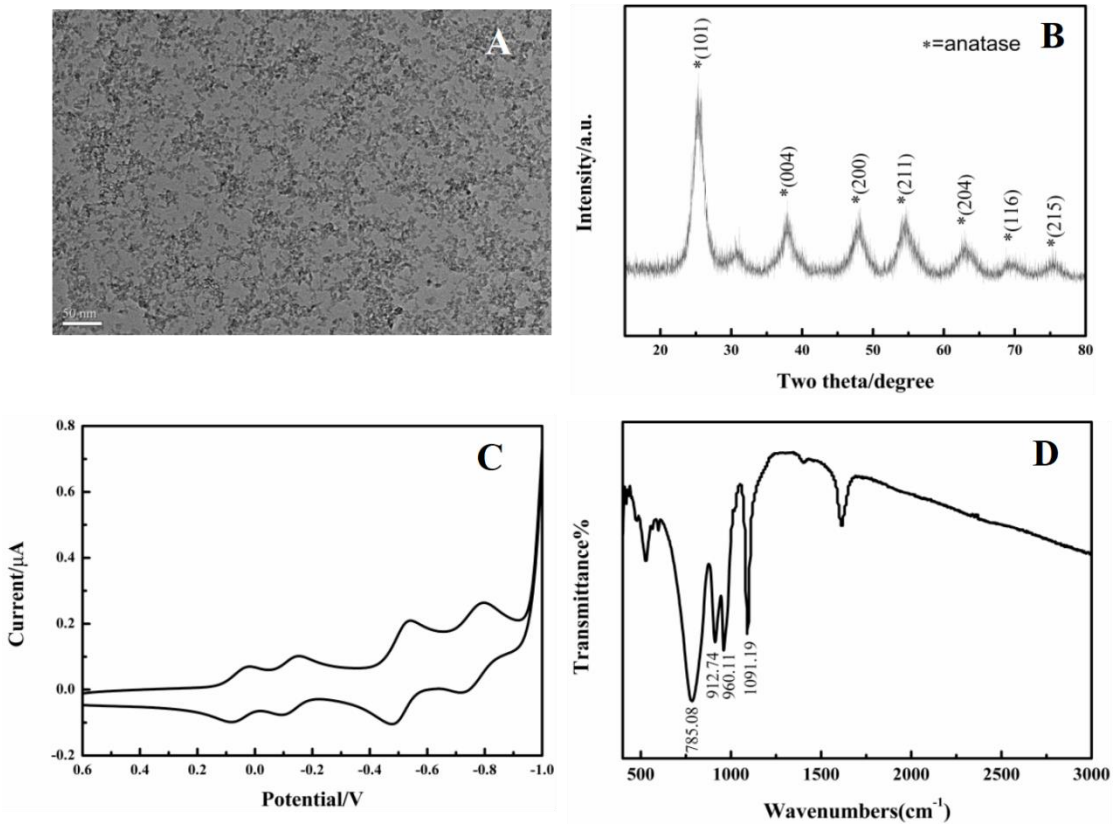

Fig.S1 Characterization of $K_6P_2W_{18}O_{62}$ and TiO_2:(A) TEM image of TiO_2 colloids;(B) XRD pattern of TiO_2 colloids;(C) Cyclic voltammograms of P_2W_{18};(D) IR spectra of P_2W_{18}.

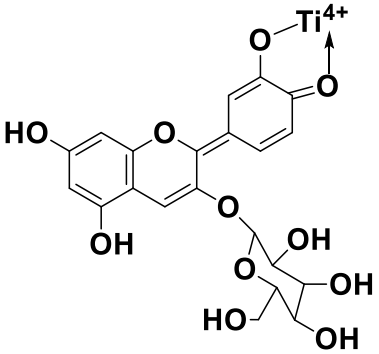

Fig.S2 Chemical structure of C3G attached to the TiO_2 surface.

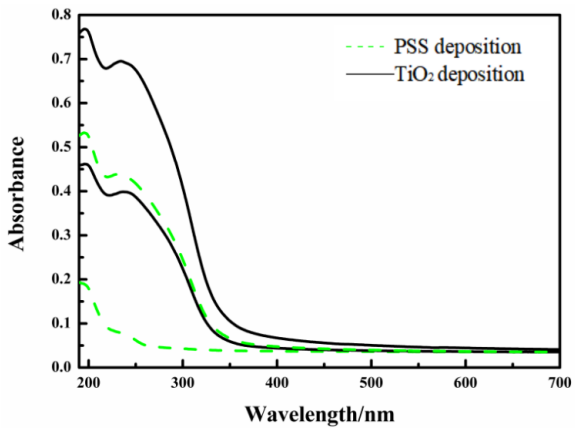

Fig.S3 UV–Visabsorption spectra of the $(PSS/TiO_2)_2$ film.

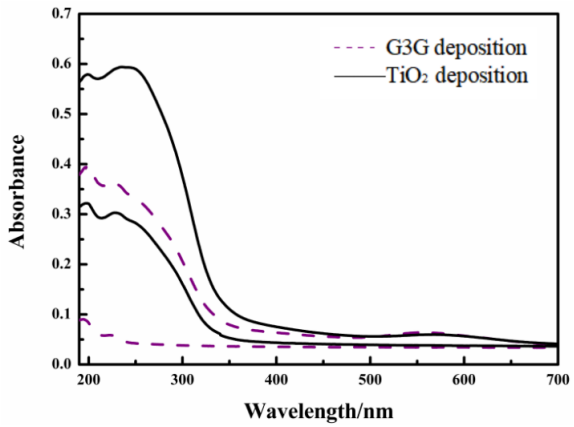

Fig.S4 UV–Visabsorption spectra of the $(C3G/TiO_2)_2$ film.

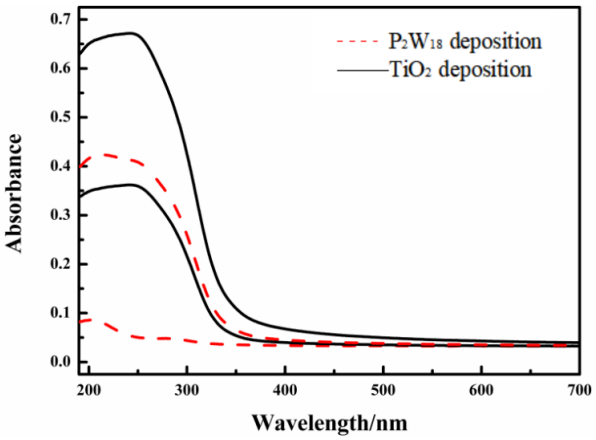

Fig.S5 UV–Visabsorption spectra of the $(P_2W_{18}/TiO_2)_2$ film.

References

1. G. Yu, J. Gao, J.C. Hummelen, F Wudi and A.J. Heeger, *Science*, 270 (1995) 1789.
2. T.R. Canterbury, S.M. Arachchige, K.J. Brewer and R.B. Moore, *J. Phys. Chem. B.*, 121 (2017) 6238.
3. L.H. Wan, L. Xu, Z.C. Mu, C.G. Wan and Z.X. Sun, *J. Mater. Chem.*, 22 (2012) 23627.
4. L.H. Wan, L. Xu, Z.X. Sun and R. Li,*Electrochim. Acta*, 155(2015) 1.
5. W.X. Zha, Z. Bai and C.Wu, *Appl. Surf. Sci.*, 25 (2010) 3493.
6. Y.C. Wei, X.X. Wu, Y.L. Zhao, L. Wang, Z. Zhao, X.T. Huang, J. Liu and J.M. Li, *Appl. Catal., B*,236 (2018) 445.
7. F. Zhou, H.B. Song, H.Q. Wang, S. Komarneni and C.J. Yan, *Appl. Clay Sci.*, 166 (2018) 9.
8. B.C. Huang, Y. Yang, X.S. Chen and D.Q. Ye, *Catal. Commun.*, 11 (2010) 844.
9. Y.X. Sun, W. Chen, X.Q. Li, Q.Y. Yu, Y.X. Zhu, Y.T. Wang, L. Chen, W. Sun, G.J. Li, Y.Y.Niu, *Int. J. Electrochem. Sci.*, 16 (2021).
10. M. Marandi and F.S.Mirahmadi, *J. Alloys Compd.*, 800 (2019) 140.
11. Y. Jia, P.B. Liu, Q.Y. Wang , Y. Wu, D.D. Cao, Q.A. Qiao, *J. Colloid Interface Sci.*,1 (2020) 585.
12. Y.H. Nien, H.H.Hsu, Z.R. Yong, G.M. Hu and J.X. Chang, *IEEE Trans. Electron Devices*, 99 (2021) 1.
13. R.R. Prabhakar, T. Moehl, S. Siol, J.Suh, S.D.Tilley, *Chem. Mater.*, 32 (2020) 7247.
14. G.G. Gao, L. Xu, W.J. Wang, Z.Q. Wang, Y.F. Qiu and E.B. Wang, *Electrochim. Acta*, 50 (2005) 1101.
15. W.Y. Tao, Z.F. Li, D.W. Pan, L.H. Nie and S.Z. Yao, *J. Phys. Chem. B*, 109 (2005) 2666.

16. K. Pawlak, M. Puchalska, A. Miszczak, E. Rosłoniec, M. Jarosz, *J. Am. Soc. Mass. Spectrom.*, 41 (2006) 613.
17. G.T.M. Silva, K.M. Silva, C.P. Silva, A.C.B. Rodrigues, J. Oake, M.H. Gehlen, C. Bohne and F.H. Quina, *Photochem. Photobiol. Sci.*,18(2019) 1750.
18. I.C. Maurya, Neetu, A.K. Gupta, P. Srivastava and L. Bahadur, *Opt. Mater.*, 60 (2016) 270.
19. M. A.M. Al-Alwani, N.A. Ludin, A.B. Mohumad, A. A.H. Kadhum and A. Mukhlus, *Spectrochim. Acta, Part A*, 192 (2017) 487.
20. R.G. Finke, M.W. Droege and P.J. Domaille, *Inorg. Chem.*, 26 (1987) 3886.
21. B. O'Regan, J. Moser and M. Grätzel, *J. Phys. Chem.*, 94 (1990) 8720.
22. S.P. Liu, L. Xu, G.G. Gao, B.B. Xu and W.W. Guo, *Mater. Chem. Phys.*, 116 (2009) 88.
23. L.Y. Zhan, J. Chen, Z.Q. Wang, R.M. Shen, N. Cui and A.D. Sun, *Int. J. Food. Prop.*, 19 (2015) 1.
24. Y. Kimura, T. Maeda, S. Iuchi, N. Koga, Y. Murata, A. Wakamiya and K. Yoshida,*J. Photochem. Photobiol., A*, 335 (2017) 230.
25. G. Calogero, A. Bartolotta, G.D. Marco, A.D. Carlo and F. Bonaccorso, *Chem. Soc. Rev.*, 44 (2015) 3244.
26. L.K. Singh, T. Karlo and A. Pandey, *Spectrochim. Acta, Part A*, 118 (2014) 938.
27. S.Q. Liu, D.G. Kurth, B. Bredenkötter and D. Volkmer, *J. Am. Chem. Soc.*, 124 (2002) 12279.
28. C.H. Sui, C. Li, X.H. Guo, T.X. Tang, Y.K. Gao, G.D. Zhou and J. Gong, J. Du, *Appl. Surf. Sci.*, 258 (2012) 7105.
29. X.F. Fu, H.P. Yang, G.H. Lu, Y.M. Tu and J.M. Wu, *Mater. Sci. Semicond. Process.*, 39 (2015) 362.
30. M.L. Arunakumari and L.G. Devi, *Environ. Sci. Water Res. Technol.*, 2 (2015) 177.
31. M.C. Long, L.H. Zheng and B.H. Tan, *Appl. Surf. Sci.*, 386 (2016) 434.
32. L.H. Wang, L. Xu, Z.X. Sun and Z.C. Mu, *RSC Adv.*, 3 (2013) 21811.
33. A. Atli, A. Atilgan, C. Altinkaya, K. Ozel and A. Yildiz, *Int. J. Energy Res.*, 43 (2019) 3914.
34. M.A. Saab, R. Abdel-Malak, J.F. Wishart and T.H. Ghaddar, *Langmuir.*, 23 (2007) 10807.
35. C.D. Grant, A.M. Schwartzberg, G.P. Smestad, J. Kowalik, L.M. Tolbert and J.Z. Zhang, *Synth. Met.*, 132 (2003) 197.
36. S. Yanagida, A. Nakajima, T. Sakaki, Y. Kameshima and K. Okada, *Chem. Mater.*, 20 (2008) 3757.
37. E.C. Prima, M.A. Qibtiya, B. Yuliarto, Suyatman and H.K. Dipojino, *Ionics.*, 22 (2016) 1687.
38. X.X. Song, R. Liu, Z.X. Sun, H.Y. Shi and L. Xu, *Mater. Res. Bull.*, 97 (2018) 326.
39. J. Marugán, P. Christensen, T. Egerton and H. Purnama, *Appl. Catal., B*, 89 (2009) 273.
40. J. Georgieva, S. Armyanov, E. Valova, I. Poulios and S. Sotiropoulos, *Electrochim. Acta*, 51 (2006) 2076.
41. R.G. Finke, M.W. Droege and P.J. Domaille, *InorgChem.*, 26.23(1987)3886.